Monte Carlo Simulation of Self-Assembly of Symmetric ABC Three-Arm Star Copolymers under Cylindrical Confinement

Jianhui Song, Tongfei Shi,* Jizhong Chen, and Lijia An*

State Key Laboratory of Polymer Physics and Chemistry, Changchun Institute of Applied Chemistry, Chinese Academy of Sciences, Changchun 130022, People's Republic of China

Received: March 30, 2010; Revised Manuscript Received: September 20, 2010

Self-assembly of symmetric ABC three-arm star copolymers confined in cylindrical nanopores is investigated by means of a lattice Monte Carlo simulation method. The dependence of morphologies on the degree of confinement and preference of pore surface is studied systematically. For the symmetric ABC three-arm star copolymers which form polygonal cylinder structures with periodic spacing L_0 in bulk, various novel structures are observed inside the nanopores. In the nanopores with a neutral surface, we find a minimum diameter value ($D_{min} \approx L_0$) under which helical arranged droplets are formed; otherwise, parallel polygonal cylinder structures are identified. By adjusting the preference between component A and the pore surfaces, a number of novel structures such as A cylinder + BC single-strand helix and complex multilayer double helices are identified. Additionally, the confinement-induced morphology transition is interpreted by the frustration parameter D/L_0.

Introduction

The self-assembly behavior of block copolymers (BCPs) has received considerable attention due to the demand for fabricated nanomaterials associated with the rapid development of nanoscience. This well-known microphase separation phenomenon is driven by the competition between the thermal incompatibility within distinct blocks and entropic effects arising from chain stretching. For the simplest diblock copolymers melts, four classical structures, including spheres, hexagonally packed cylinders, lamellae, and complex bicontinuous gyroids, have been identified both experimentally and theoretically.[1,2] These microscopic ordered structures formed in bulk are of great interest in many technical applications, e.g., templates for nanowire fabrication, nanolithography, and high-density magnetic data storage media.[3] Recently, many novel self-assembled morphologies which are not accessible in bulk melts[4,5] and under one-dimensional confinement have been produced by imposing a two-dimensional (2D) confinement with a cylindrical channel boundary.[3,6−8] Under a confined environment, the structural frustration, the surface−segment interaction energy, and the confinement-induced entropy loss combine to induce morphological diversity.[4] Exploring the self-assembly phase behavior of block copolymers under a 2D confinement environment not only offers a new approach to acquire novel ordered mesostructures that are not accessible in bulk or under 1D confinement but also is of great fundamental importance in polymer science.

For self-assembly under 2D confinement, the confinement effect can strongly restrict the freedom of motion of copolymer chains, while surface interaction can significantly influence the orientation of microdomains formed by each component. Thus, both nanopore size and surface preference are expected to tune the self-assembly of block copolymers. Recently, the self-assembly of block copolymers in a confined environment has received much attention both experimentally and theoretically. By employing nanoscale cylindrical pores produced in alumina membranes, Russell and co-workers systematically studied the 2D confinement-induced morphologies of both symmetric and asymmetric polystyrence-*b*-polybutadiene (PS-*b*-PBD) diblock copolymers. They observed a series of novel morphologies such as multiple concentric cylindrical barrel structures,[9,10] stacked toroids,[11] helical arranged spheres,[11] and a stacked disk[9] as well as helical structures.[12] When the pore diameter D is relatively wide (larger than the bulk period L_0), concentric barrel and axial cylinder structures are observed. When the pore diameter D is relatively narrow or highly incommensurate with the bulk period L_0, some unusual morphologies such as helical and stacked toroid structures are observed. Theoretically, the Monte Carlo simulation technique has proved to be a powerful tool to predict the morphological behavior of block copolymers under a 2D confinement environment.[4,5,13−17] For symmetric diblock copolymer melts, besides confirming the multiple concentric lamellar structure and stacked disk observed in experiments, the simulations predicted a number of novel structures, including porous lamellae, axial lamellar structures, and single-strand and double-strand helical structures.[13,14,16] In order to elucidate on the formation of the novel ordered structures within the framework of Monte Carlo technique, Yu et al. employed a simulated annealing method to systematically examine the 2D confinement-induced morphology of asymmetric diblock copolymer melts.[4] They observed many interesting structures that depend on the pore size and surface interactions. They also revealed that the morphology has a tendency to transition from helices to toroids to spheres by tightening the degree of confinement. Sevink et al. used dynamic density functional theory to study the self-assembled morphology dependence of symmetric lamella-forming diblock copolymers on cylindrical confinement.[18] Li and Wickham used real-space self-consistence field theory (SCFT) to construct the phase diagram of diblock copolymers confined in cylindrical nanopores in two-dimensional space,[19] and subsequently their work was extended to three-dimensional space to explore equilibrium phase structures in order to give a direct comparison with experimental findings.[20] This numerical prediction confirmed the results reported by Yu

* To whom correspondence should be addressed. E-mail: tfshi@ciac.jl.cn or ljan@ciac.jl.cn; tel: +86-431-85262137; fax: +86-431-85262969.

10.1021/jp102863w
Published on Web 11/17/2010

et al. in ref 4. In the intermediate segregation region, Chen and co-workers utilized SCFT to investigate the self-assembled microstructures of asymmetric cylinder-forming diblock copolymers confined in cylindrical pores.[21] The prediction was in good agreement with the available experimental results.

For 2D confined self-assembly, most studies were devoted to the copolymers with linear architecture, including diblock copolymers,[4,9−23] linear triblock copolymers,[5,24] and diblock copolymer blends.[25,26] Previous studies have shown that the copolymers with nonlinear architectures can generate some unique ordered structures that are not observable in linear systems. In bulk melts, ABC triblock copolymers have attracted much attention due to their ability to self-assemble into various fascinating ordered structures. Compared with diblock copolymers, the addition of the third component brings two significant influences to the self-assembly behaviors of ABC triblock copolymers. First, as the number of blocks increases from two to three, complexity and diversity of self-assembled mesophases might be expected because of introducing more interaction and structure parameters. Second, it is possible to construct a chain with distinct topological architectures, for instance, linear ABC or star-shaped ABC copolymers. Because of the synthetic difficulties of star-shape ABC copolymers, early studies have mainly focused on linear ABC triblock copolymers.[27−31] Recently, development of synthesis techniques has enabled researchers to readily obtain and characterize star-shaped copolymers.[32−41] In the meantime, numerical efforts have been made to uncover the phase behavior of star-shape ABC copolymers.[42−47] For example, Gemma and co-workers employed Monte Carlo simulation methods to examine the morphological behavior of star-shaped ABC copolymers, varying the block length ratio of 1:1:*x*.[43] They observed a number of novel morphologies such as lamellae + spheres, lamellae + cylinders, columnar disks, and the typical cylindrical phases with polygonal cross-sections that are denoted as a set of integers [*k*.*l*.*m*].[43] The integers within the bracket represent the total number of contact interfaces within the corresponding polygonal patterns. On the basis of a real-space implementation of the self-consistent field theory, Tang et al. constructed the two-dimensional phase diagram of star-shaped ABC copolymers in the intermediate segregation regime.[46] These previous studies clearly indicate that the geometrical constraint arising from the junction point connecting three distinct blocks may induce many novel structures that are not accessible in the bulk melts of copolymers with linear architecture. For instance, when both the volume fraction and repulsion energies of the three species are comparable, the linear ABC triblock copolymers self-assemble into lamellar phases,[31] while the symmetric star-shaped copolymers form a unique cylindrical phase with [6,6,6] polygonal cross-sections[43] as illustrated in Figure 1. Note that three components in a symmetric star-shaped ABC copolymer are spatially equivalent. However, for linear ABC triblock copolymers, the lamellar structures show different phase spacing thickness because of the absence of the spatial equivalence.[31] Since star-shaped ABC copolymers show a large number of new morphologies that are not observed in linear ABC triblock copolymers as mentioned above, it is expected that the corresponding confined self-assembly might lead to different ordered structures.

In this paper, we employ a Monte Carlo simulation method to investigate the self-assembly behavior of the symmetric star-shaped ABC copolymer confined in a cylindrical nanopore. The Monte Carlo simulation technique has proved to be one of the most successful tools for the prediction of the morphological

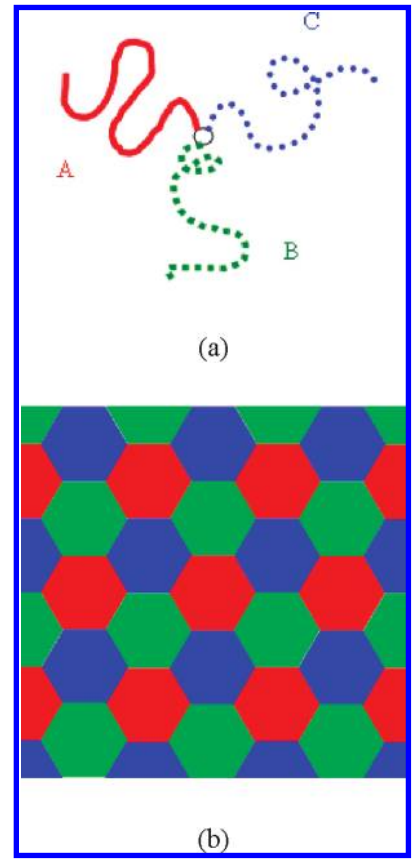

Figure 1. Schematic graphs of (a) a star-shaped ABC copolymer consisting of a junction point and three different arms; (b) a typical [6.6.6] polygonal cylinder pattern.

behavior of block copolymers confined in cylindrical nanopores.[4,5,13−17,22−24,26] Although a large number of studies have been carried out on the two-dimensional confined self-assembly of linear copolymers, the dependence of morphology on chain architecture is not clearly understood. One pioneering work on this topic by Xu et al. employed an SCFT approach to construct the phase diagram of the 2D-confined self-assembly of asymmetric ABC star copolymers by comparing the free energy of different equilibrium microstructures.[48] Specifically, they chose star polymers with an asymmetric arm length ratio that forms hierarchical lamella in bulk. Owing to the variety and complexity of star-shaped copolymers, the confined morphology depends on a number of parameters such as arm length ratio, interaction strength between distinct blocks, and surface preference. A thorough study on such a complex system requires a great deal of experimental and theoretical effort. For the purpose of more generally addressing the 2D-confined self-assembly behavior of ABC star copolymers, we focus on the morphological behavior of the symmetric star-shaped ABC copolymers confined in a nanocylindrical pore. By examining this simplest case of star-shaped ABC copolymers, we may achieve a preliminary understanding that might provide better access to explain more complex phenomena existing in this system. In our simulations, the dependence of morphology on the pore size and surface interaction has been systematically examined. We observe a variety of novel structures that have not been found in the 2D-confined self-assembly of linear copolymers. Our results may provide a preliminary understanding of the self-assembled structures of complex copolymers subjected to 2D confinement.

Model and Simulation Method

The computer simulations performed in our studies are based on an improved eight-site bond fluctuation model[49] and volume diffusion algorithm.[50] The model is described briefly below, and the detailed description can be found elsewhere.[49,51,52] In this model, one segment occupies a cube consisting of eight lattice sites. The excluded volume effect is satisfied by prohibiting one cube occupied by two segments simultaneously, and the backbone connectivity is maintained by selecting appropriate bond lengths. The allowed bond length is set to 2, $5^{1/2}$, $6^{1/2}$, 3, and $10^{1/2}$ lattice units. The Metropolis rule is employed to judge the acceptance of any attempted movement. Compared with the simple single-site model,[52] the advantage of the eight-site model is reflected by affording 108 possible bond vectors and 87 different bond angles.[52] The simulation results obtained in the eight-site model are much closer to those in continuous space, which is exactly the situation that occurs in real experimental systems. Furthermore, the existence of abundant possible bond angles enables us to simulate star-shaped branch molecules and semiflexible polymers.[54]

In this study, the symmetric $A_6B_6C_6P_1$ star-shaped copolymers with a volume fraction of 0.9 are considered. Here, P represents the junction point which is necessary to connect the three distinct blocks on the discrete lattice while retaining the symmetry of the star polymer chain. The remaining volume fraction of the lattice is occupied by vacancies. Two segments can interact only when the distance between them is no more than $6^{1/2}$, which ensures that the first peak of the correlation function is encompassed within the range of potential.[54] The interaction energy between the same kind of species is set to zero. Interactions among the different kinds of segments are set as follows: $\varepsilon_{AB} = \varepsilon_{AC} = \varepsilon_{BC} = \varepsilon_{AP} = \varepsilon_{BP} = \varepsilon_{CP} = 1.0k_BT$. This set of interactions maintains an ideal symmetric repulsion potential in the system. In order to ensure that the ordered morphologies are stable, we perform a simulated annealing procedure that involves a gradual increase in interaction energy from 0 (i.e., athermal state) to $1.0k_BT$ in steps of $0.1k_BT$. For the preferential surface cases, the interaction between A-type segments and the surface ε_{AS} is set to $1.0k_BT$ (repulsive) and $-1.0k_BT$ (attractive), respectively. Interactions between other kinds of segments and the pore surface are all set to zero.

An impenetrable cylindrical boundary with a diameter D is applied on the $X-Y$ plane while a periodic boundary condition is used on the Z direction. A series of pore diameter values are examined in our simulations in order to explore the dependence of morphology on confinement degree. The nanopore boundary is realized in such a way that if the distance between one lattice site and the central point on the same $X-Y$ plane is larger than $D/2$, this site is regarded as a hard wall and thus any attempt to move toward this site is prohibited. Due to the discreteness of lattice model, when the nanopore size is relatively small, the shape of the boundary can be accurately described as a polygonal column rather than a cylinder. The length of the cylindrical pore L is 84 lattice units. Because in the present study each segment occupies one cube, for convenience, all the length values in the following context are denoted in units of the lattice cube, which should be half of the value represented in lattice units. For example, the length of nanocylindrical pores L is equal to 42 in units of the cube. At each annealing step, we perform 1×10^6 Monte Carlo steps (MCS) to equilibrate the system. MCS is defined as the time spent for all the segments within the simulation box that have a trial move on average.

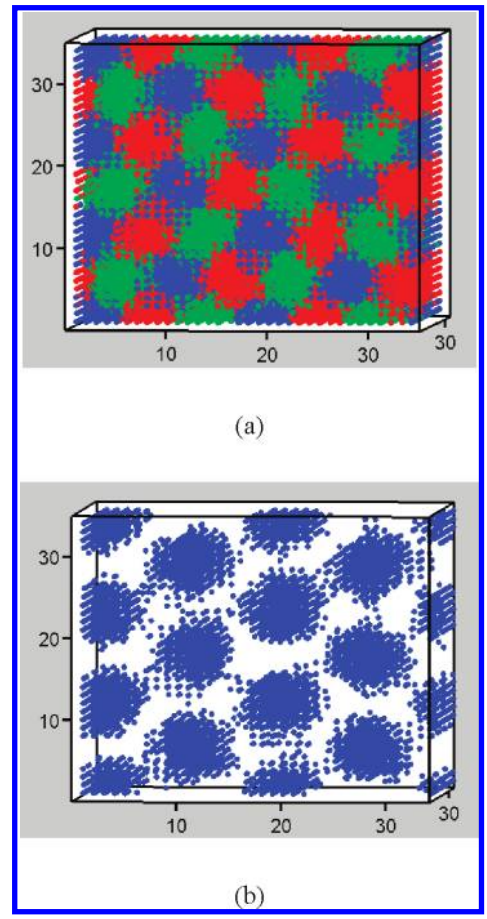

Figure 2. Morphology snapshot of symmetric ABC star polymers in a simulation box of axial length $L_b = 34$. (a) All three components are displayed; (b) only C-type segments are displayed. The red, green, and blue sites represent A, B, and C segments, respectively.

Results of Discussions

Generally, the confinement degree of the cylindrical pores is quantified by the dimensionless parameter D/L_0, which is the ratio between the pore diameter and the bulk period of symmetric ABC star copolymers. In order to determine the bulk period L_0, we first perform the simulations of symmetric ABC star copolymers in bulk, varying the box length $L_b = 32$, 34, and 36. When L_b is fixed at 34, the typical [6.6.6] cylindrical phase parallel to one axis (X, Y, or Z) is observed as shown in Figure 2. In the cubic lattice, the orientation of self-assembled microdomains adjusts so that the bulk periodic spacing can match the dimension of the simulation box. Figure 3 shows the segment density distribution along the axis on the cross-section of the cylindrical phase. From Figure 3, it can be seen that the simulation box contains four periods on the direction parallel to the box axis, indicating that the spacing between the centers of two adjacent cylinder microdomains L_A can be estimated as: $L_A = L_b/4 = 8.50$. Then, through a simple geometrical analysis, the bulk period L_0 can be calculated as: $L_0 = 2L_A/3^{1/2} \approx 9.82$ in units of segment cube. In the following, the self-assembled structures are displayed as a function of the confinement degree D/L_0. This work examines the dependence of morphology on both the confinement degree and surface interactions inside the cylindrical pores with a diameter of a few L_0.

Because the three arms of the ABC star polymers we studied are spatially equivalent, it is of interest to reveal how the confined space, i.e., the cylindrical pore, is divided by these three equivalent components under equilibrium conditions. In

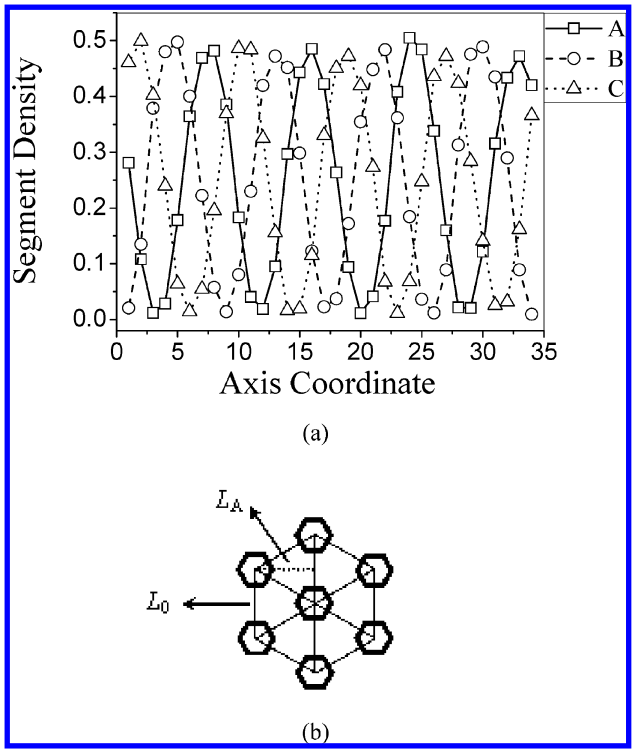

Figure 3. (a) Segment distribution plot along the pore axis. (b) Schematic illustration of two periods correlated to the polygonal cylinders.

this case, no preference between the pore surface and the polymer segments is allowed. So far as we have known, few studies have focused on such an issue. In our simulations, a number of novel structures are presented in Figure 4a, including discrete cylinders with single-strand helical arrangements (n1), a single layer of alternate cylinders embedded in alternate lamella (n2), distorted polygonal cylinders perpendicular to the pore surfaces (n3), and perfect polygonal cylinders perpendicular to the wall surfaces (n4). Four kinds of self-assembled structures observed in this case are labeled as ni (i = 1, 2, 3, 4) which will be employed to represent the corresponding morphology in the following discussions. For the pores of narrow sizes $D/L_0 \approx 0.61-0.81$, discrete cylinders with single-strand helical arrangement (n1) are formed where cylinders are aligned on the direction parallel to the wall. Interestingly, by combining any two components, a single helix-like structure is observed. In the asymmetric diblock system, Chen et al. reported a similar morphology inside a relatively small pore, which might be regarded as an analogue formed in a two-component system.[21] When $D/L_0 \approx 1.02$ or 1.22, a one-layer polygonal cylinder structure perpendicular to the axis of the nanopore is formed. The row of the alternate polygonal cylinders formed by A, B, and C components lies across a certain diameter cross-section of the cylindrical pores, which is surrounded by two symmetric shells consisting of alternate lamellae. A further increase of the pore size leads to a distorted polygonal cylinder structure denoted as n3. This irregular morphology persists until $D/L_0 <$ 1.83, suggesting that confinement-induced structure frustration leads to such a morphology transition. When $D/L_0 \approx 1.83$, polygonal cylinder structures with two layers appear (Figure 4, n4). For the largest pore size we used, $D/L_0 \approx 3.05$, seven layers of cylinders are observed (not shown). In general, in the case of a relatively large pore size, the ABC star polymers tend to form polygonal cylinder structures perpendicular to the pore axis, whereas by tightening the cylindrical pores, helical arranged cylinders become favorable.

On the basis of the above observations, it would be interesting to make a direct comparison with the corresponding morphologies of symmetric *AB* diblock copolymers confined in neutral cylindrical pores. In the case of a symmetric diblock, stacked-disk structures where lamellae are perpendicular to the pore surface are highly favored, especially for small pore size and moderate interaction strength between two distinct blocks. Although some complex morphologies such as various helical structures were also reported earlier by MC simulation,[14,15] these complex structures may be attributed to the incommensurability between the pore length and the lamellae domain spacing suggested by both SCFT calculation[56] and cell dynamic simulations.[55] Pinna et al. proposed that the stability of microphase-separated morphologies of confined symmetric diblock copolymers are determined by the competition between the surface and incommensurability effect, while the former factor scales with the surface area and the latter scales with volume of the pore system. Such a competition still holds for the symmetric ABC star polymers in a neutral cylindrical pore, which results in a discrete cylinder structure (n1) parallel to the wall at a small diameter and then transforms to a bulk-like polygonal cylinder structure (n4) with an orientation perpendicular to the wall with increasing pore size. The formation of n2 and n3 structures can be rationalized, as the pore diameter resides in an intermediate region where neither surface nor bulk effect can prevail. Compared with the morphologies of diblock copolymers at small diameters, one pronounced feature of the structures formed by star polymers is no individual component, e.g., block A, B, or C, can occupy an entire cross-section of the cylindrical pore, indicating that the chain architecture plays a crucial role in the formation of an ordered phase in confined space. Figure 4b shows the typical axial segment distribution function (definition see below) of the star polymers in nanopores. The alternate sinusoidal curves are similar to that observed in bulk melts (see Figure 3a), reflecting that the periodicity is maintained along the pore axis for the purpose of minimizing the free energy of the system. While at small diameter two components of the symmetric diblock can form alternated lamellae (stacked-disk) perpendicular to the pore surface provided that ordered phases are spatially equivalent, the symmetric ABC star polymers require an additional symmetry degree of freedom, which rationalizes the formation of the unique helix-arranged cylinder structures as shown in Figure 4a (n1).

Although for relatively large pore size ($D/L_0 \geq 1.83$) the system facilitates the formation of polygonal cylinders perpendicular to the axis of the cylindrical pore, the local arrangements of the polygonal cylinders differ in the confinement degree. As shown in Figure 5, two typical cylinder packing patterns are classified at $D/L_0 \approx 2.44$ (Figure 5a) and 2.65 (Figure 5b). For the convenience of description, according to the relationship between the array line of cylinders and the pore axis, the pattern styles shown in Figure 5a and 5b are referred to as parallel and perpendicular packing, respectively. Although we are not able to directly compare the free energy of these two packing styles, a simple comparison of the contact area on the edge of the polygonal cross-section in the vicinity of the pore surface might indicate their stability. It is quite obvious that two parallel undulated pillar structures with periodic phases cover the pore surface on the edge of the cross-section of [6.6.6] polygonal cylinder phase. For the parallel packing (Figure 5a), each microdomain on the pillar has to interact with four distinct adjacent phases while the total number of phase interfaces becomes three in the case of the perpendicular packing style. Consequently, for the purpose of minimizing the energy penalty,

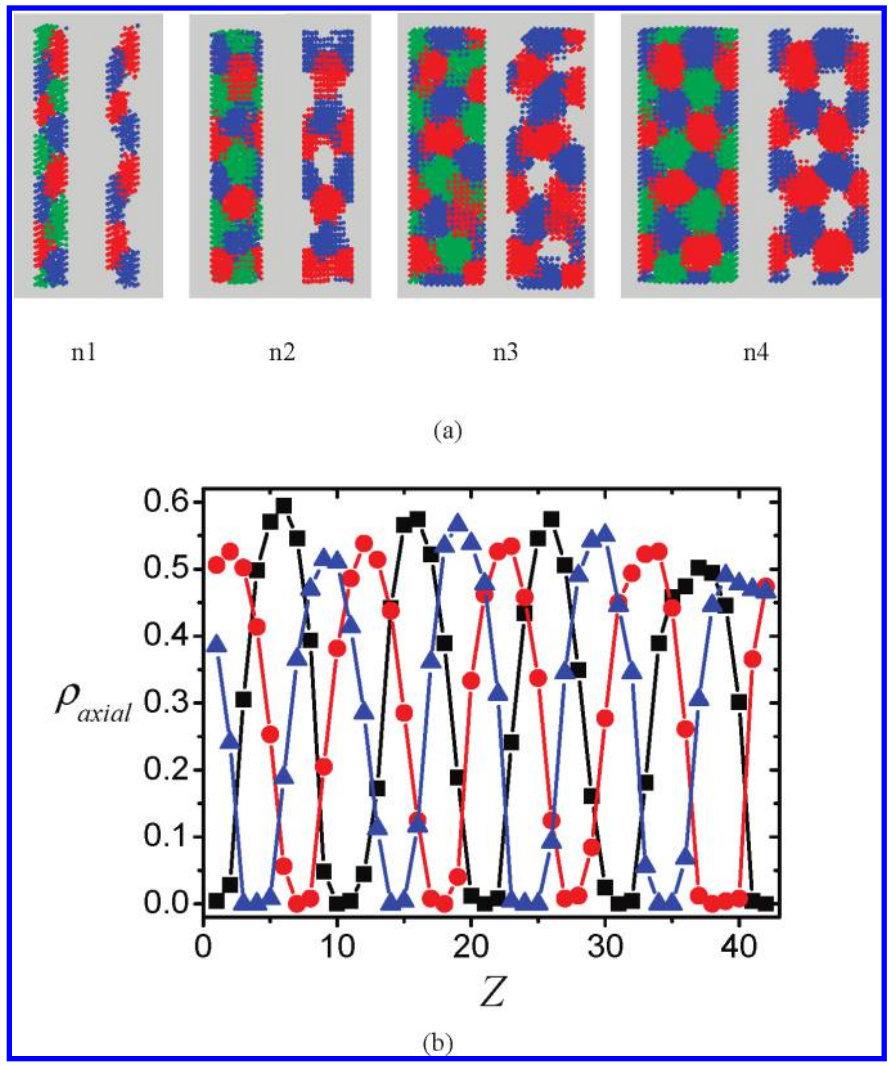

Figure 4. (a) The snapshot of the typical morphologies formed under the neutral pore surface. (b) The typical axial segment distribution function.

the polygonal cylinder structure may tend to adopt the perpendicular packing style. Note that two packing styles correspond to the respective lattice spacing along the radial direction of the nanopore, i.e., L_0 for the parallel packing whereas L_A for the perpendicular situation. Replacing L_0 with L_A in the confinement parameter, we find that the perpendicular packing style is preferable at $D/L_A \approx 3.06$ while the parallel one is obtained at $D/L_A \approx 2.82$. That is, the system favors the perpendicular packing when D/L_A is close to an integer for the relatively wide pores; otherwise, the packing pattern may rotate to relieve the space frustration arising from boundary confinement.

Next, we investigate the surface field effect on the morphology behavior. The interaction strength between the pore surface and polymer (A blocks) interaction ε_{AS} is fixed at $-1.0k_BT$ (strongly attractive) or $1.0k_BT$ (repulsive). The typical morphologies observed under the attractive surface field are presented in Figure 6. Because preferential affinity forces A blocks to be in contact with the pore surface to form a wetting layer, a circular lamellar shell close to the pore surface always exists for all pore sizes we examined. Noted that there are not sufficient A-type segments to cover to wall surface at small pore diameters ($D/L_0 < 1.43$). For the purpose of simplifying description, we omit addressing this shell in the following part. The transition sequence of morphologies along with increasing the pore diameter can be depicted in terms of the A-type domain structures within the inner area of the pore. When the pore diameter is small ($D/L_0 \leq 1.43$), alternate stacked disks (Figure 6 a1) are formed without any aggregation of the surface-attractive A-type segments. Upon further increasing the pore diameter, we observe a sequence of A-type domains formed within the central region of the cylindrical pore, ranging from droplets (see Figure 6, a2, $D/L_0 \approx 1.63$), a discontinuous cylinder (a3, $D/L_0 \approx 1.83$), a continuous cylinder (a4 and a5, $D/L_0 \approx 2.04-2.24$), and discontinuous toroid structures (a6, $D/L_0 \approx 2.85-3.05$). At $D/L_0 \approx 2.24$, two possible morphologies coexist in our simulations as displayed in Figure 6b and 6c. Between the outer lamellar layer near the pore surface and the central cylinder, components B and C can separately form either a single helix (Figure 6c) or piled toroid structure (Figure 6, a5), which indicates that the energies related to the two morphologies are comparable. The above evolution of structures can be explained as follows. At small diameters all the surface-attractive segments are induced to wet the pore surface in order to lower the total energy of the system. Upon a slight increase in the pore diameter, the region near the pore surface cannot accommodate the excess A-type segments, which tend to move to the inside of the pore and thus yield some small droplets. As a result of larger aggregations of A-type segments caused by a further increase in the pore diameter, the transformations from droplets to cylinder and then to toroid structures are expected.

To better understand the morphologies under the surface field, the axial and radial segment distribution density functions are

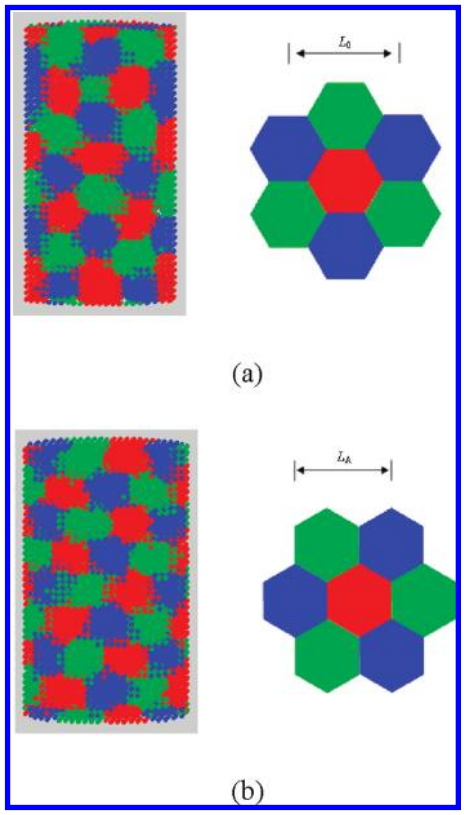

Figure 5. Schemes of two possible packing styles in polygonal cylinder structure perpendicular to the pore axis.

also employed to characterize the structures. The definitions of the two above functions are:

$$\rho_{\text{axial}} = m_z^i / m_z^{\text{total}} \tag{1.1}$$

$$\rho_{\text{ra}} = m_r^i / m_r^{\text{total}} \tag{1.2}$$

where m_z^i and m_z^{total} denote the number of i-type segments and total number of sites on a certain cross-section perpendicular to the pore axis, respectively. And m_r^i and m_r^{total} denote the corresponding variables within a certain layer of a series of concentric shells. The radial segment distribution functions are displayed in Figure 7. It can be seen that the increase of pore sizes results in the evolution of multilayer structures, which is in agreement with the tendency observed in the morphology snapshots shown in Figure 6. Because of the existence of the attractive pore preference, the outer two layers are fully occupied by the A-type segments. The formation of the multilayer structures arises from the competition of chain stretching energy and the pore surface affinity to one block. The maximum lamella spacing is no more than five lattice units as shown in Figure 7, which is determined by the block length of the star polymers. When such a limit is reached, one part of surface-attractive segments is required to move from the vicinity of the pore surface to the inner area to reduce the energy loss from chain stretching. These novel structures we observed are significantly different from those obtained in $A_mB_mC_m$ linear triblock copolymers, which prefer to induce multilayer curved lamellae.[5] This suggests that the variation of the chain architecture can be a practical way to tailor the ordered structures of copolymers under a confined environment.

Another area for investigation is the periodic spacing of the alternate stacked disk or toroid, which can be estimated through the axial segment distribution function. As shown in Figure 8,

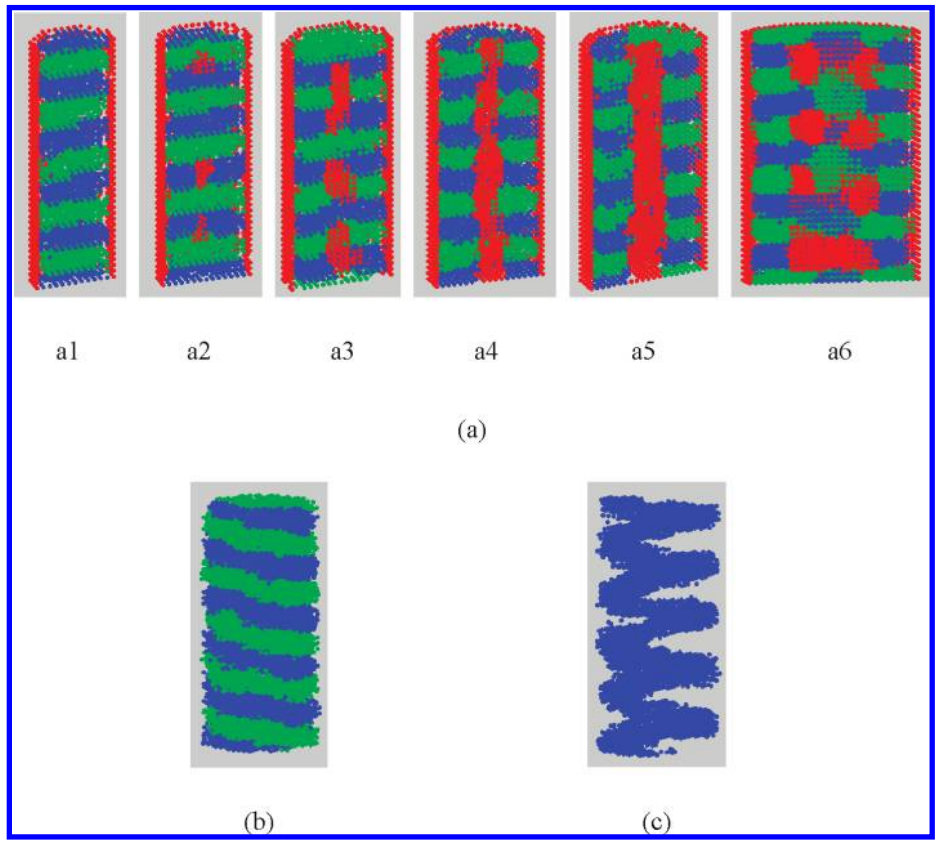

Figure 6. (a) The snapshot of the typical morphologies formed under the A-attractive surface. (b) Only B and C segments are displayed for the a5 structure. (c) Only C segments are shown.

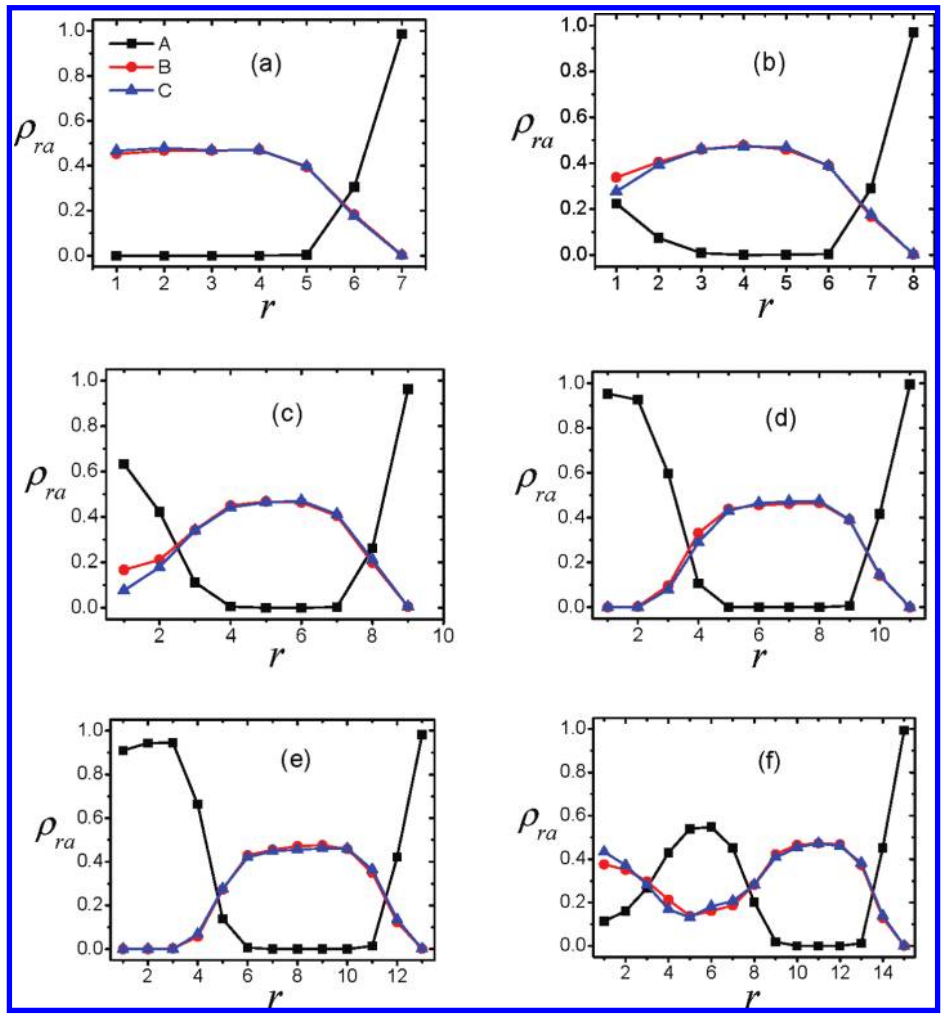

Figure 7. The radial segment distribution functions at different confinement degrees. The corresponding values of D/L_0 are (a) 1.43, (b) 1.63, (c) 1.83, (d) 2.04, (e) 2.24, (f) 3.05.

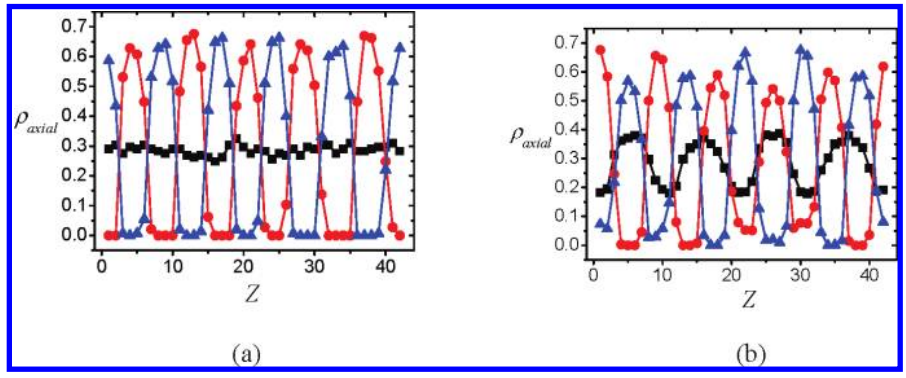

Figure 8. The axial segment distribution functions at $D/L_0 \approx 1.43$ and 3.05.

under various pore diameters, it is evident that the system contains five periodic domains, indicating that the spacing of the stacked disk or toroid is always equal to L_A rather than L_0. The reason for this deviation from bulk periodic spacing is clear after we compare the spacing of the ordered domain (B + C stacked disk or A toroid) inside the wetting layer near the pore surface. Because blocks B and C connect with A-type segments form the thin wetting layer, they tend to align to form an alternate structure with a smaller lamellar spacing. While the central A cylinder transforms to a discontinuous A toroid at $D/L_0 \approx 2.85-3.05$, the number of the periodic A toroids is reduced from five to four, suggesting that, away from the surface, the bulk effect dominates and therefore the bulk periodic spacing still holds.

In the case of the A-repulsive surface, A blocks are forced to be away from the pore surface. The morphologies observed in this case are summarized in Figure 9. At the smallest pore diameter $D/L_0 \approx 0.61$, the r1 structure (outer BC single helix + inner A cylinder) is formed. When $D/L_0 \approx 0.81-1.63$, the central A cylinder is surrounded by alternate pillars with different periodic spacings (from two to four domains, as shown in Figure 9, r2, r3, and r4) consisting of blocks B and C. The variation of the number of periodic domains consisting of blocks B and C results from the chain packing frustration originating

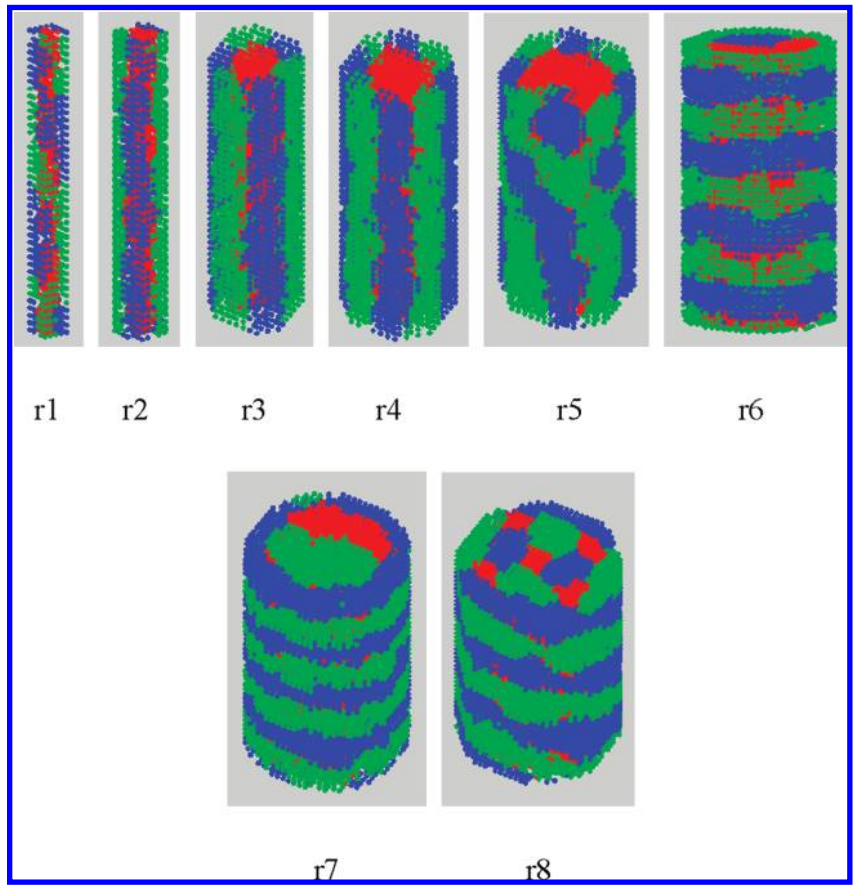

Figure 9. The typical morphologies formed for the case of an A-repulsive surface.

from the confinement degree D/L_0. We will give more details on this issue below. As the pore diameter is increased up to $D/L_0 \approx 2.04$, the r4 structure starts to be distorted and the BC wave lamellae are formed. All the above structures may be regarded as two-layer structures, i.e., an inner part composed of an A cylinder and an outer shell consisting of BC alternate lamellae. For D/L_0 within the region from 2.24 to 3.05, we obtained more complex three-layer (Figure 9, r6, r7) or four-layer (Figure 9, r8) structures where the A-type domains are embedded within the inner and outer layers of components B and C. In order to clearly identify the inner structure of these complex phases, we present the half-section and single-component view of morphology snapshot as shown in Figure 10. We describe these complex morphologies in terms of the individual layers with a sequence from outer layer to inner layer: r6 = BC alternate stacked-toroid (outer layer) + A single helix (middle layer) + BC alternate interdigitated-disk (inner layer), r7 = BC alternate-toroid + A tilted toroid + BC alternate interdigitateddisk, r8 (four layers) = BC double helix + A perforated circular lamella + BC double helix + A cylinder. Although the A-type segments have strong repulsive interaction with the pore surface, they do not always stay in the central region of the cylindrical pore. The reason becomes clear after we compare the corresponding radial segment distribution functions as shown in Figure 11. As mentioned above, at small diameters (distribution data not shown), only two radial layers are observed and A-type segments reside in the central area of the pore due to the repulsive surface. When the two-layer structure transforms to the three-layer structure, the A-type domain is wrapped by the inner and outer BC shells (Figure 11a), suggesting that maintaining a two-layer structure brings a larger stretching penalty at this pore size. As the pore diameter is further increased, while the system undergoes a transition from three-layer to four-layer structure, the distance between the two distribution peaks of the A-type segments is close to 10 lattice units which is bulk period L_0 (Figure 11b), suggesting that the separation of layer structures intensely depends on the bulk period. Consequently, the morphology transition sequence shown above may be interpreted as a competition between the surface field and bulk period. As a result of the repulsive surface, the density of the A-type segments near the wall is close to zero. At small diameters, because the system does not suffer too many penalties arising from the chain stretching, A-type segments only reside in the center of the pore and form a cylinder parallel to the wall. Upon an increase in the pore diameter, the bulk effect becomes dominant and then induces a multilayer concentric structure governed by the bulk periodic spacing.

A greater variety of morphology found in our simulations is summarized as a function of D/L_0 in Figure 12. In the neutral surface case, as long as the diameter is not very small, the ABC star polymers facilitate the formation of polygonal cylinder structures perpendicular to the pore axis. For the case of the selective surface, the system shows the ability to self-assemble into richer structures than those formed in the case of the neutral surface. Previous studies have proven that the confinement-induced morphology of diblock copolymers can be understood based on the frustration parameter D/L_0.[4,58] This parameter can also be used to understand the morphology transition in the star polymers we studied. However, due to the complexity of three components associated with the star polymers, the effect of D/L_0 on the structure evolution has to be considered in a more complicated manner. Here, in order to clearly show the role of this frustration parameter, we investigate the number of the outer

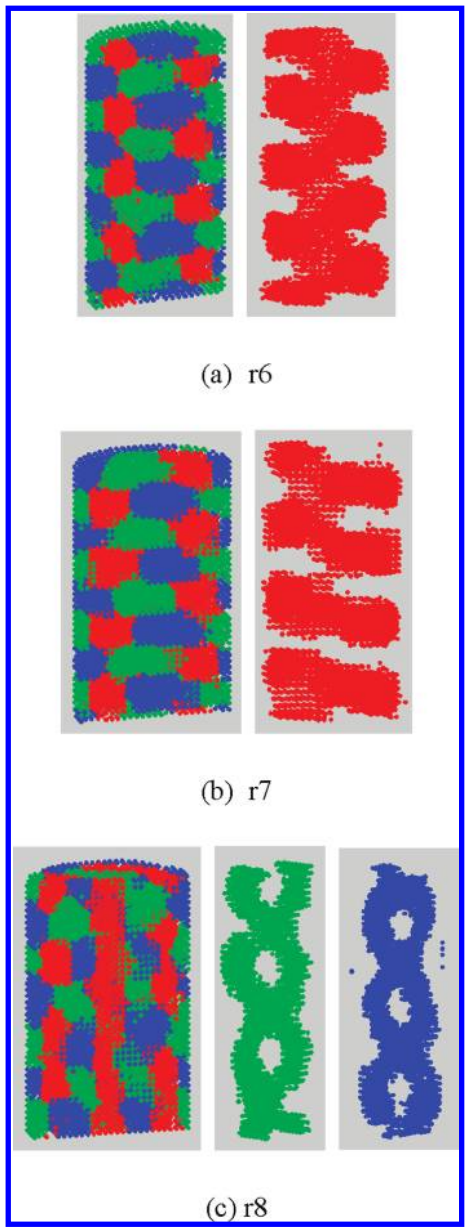

Figure 10. The section view of a single-component snapshot of (a) r6 structure, (b) r7 structure, and (c) r8 structure.

alternate BC lamellae from r2 to r4 based on a simple geometric analysis. In Figure 13, each picture represents one cross-section of the cylindrical pore. The outer circle marks the boundary of the pore, and the inner geometric graph shows the domain distribution of one component (B or C). According to the number of the outer alternate lamellae observed in the corresponding morphologies, we use the three graphs in Figure 13

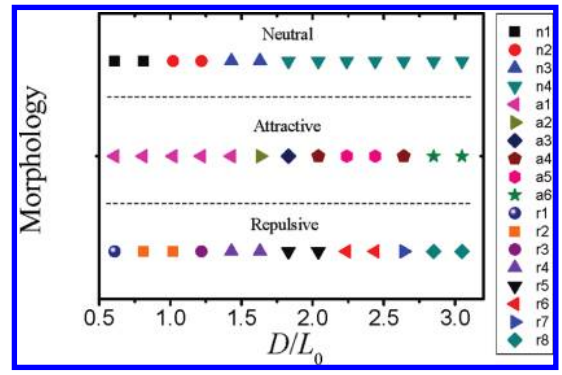

Figure 12. The phase diagram of symmetric ABC star polymers presented as a function of D/L_0.

to represent the relevant domain distribution: a diameter line (two periods, Figure 13a), a triangle (three periods, Figure 13b), and a square (four periods, Figure 13c). Note that the side length of each graph stands for the spacing between the same types of domain. Assuming the morphology transition is determined by the frustration parameter D/L_0, the values of this parameter should satisfy the following relationship: $D/L_0 = 1.0$ (diameter line), $D/L_0 = 2/3^{1/2} \approx 1.1$ (triangle), $D/L_0 = 2/2^{1/2} \approx 1.4$ (square). These predictions are congruent with our morphologies where lamellae with two, three, and four periods are formed at $D/L_0 \leq 1.02$, $D/L_0 \approx 1.22$, and $D/L_0 \geq 1.42$, respectively. These results confirm that the confined morphology of the symmetric ABC star polymer may also be understood on the basis of the frustration parameter D/L_0.

Conclusion

In this paper, the confined morphologies of the symmetric star-shaped ABC copolymers in cylindrical nanopores were investigated by Monte Carlo simulations. The effects of the pore size and surface−polymer interaction have been examined systematically. In our simulations, numerous novel morphologies including helical arranged ABC cylinders, central A cylinder + outer BC single helix, A cylinder and perforated shell + BC inner and outer double helices are identified. The variety of the morphologies can be considered as a result of the competition between the surface effects due to the pore confinement as well as surface affinity and bulk effect. As long as the pore diameter is not very small (comparable or larger than L_0), the morphology transition may also be understood based on the frustration parameter D/L_0.

Although the ABC star polymers with identical arm length and symmetric interaction potential represent the simplest morphology among complex chain architectures, they exhibit a greater variety of novel structures that are not accessible in linear ABC triblock copolymers. Our results suggest that the control of self-assembled ordered structures can be enhanced

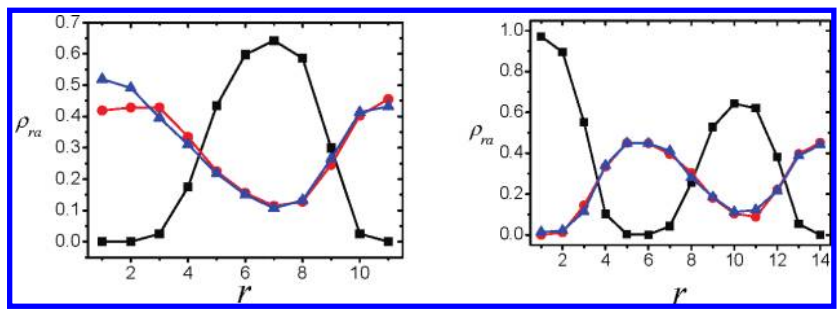

Figure 11. The radial segment distribution function under the A-repulsive surface at $D/L_0 \approx 2.24$ and 2.85.

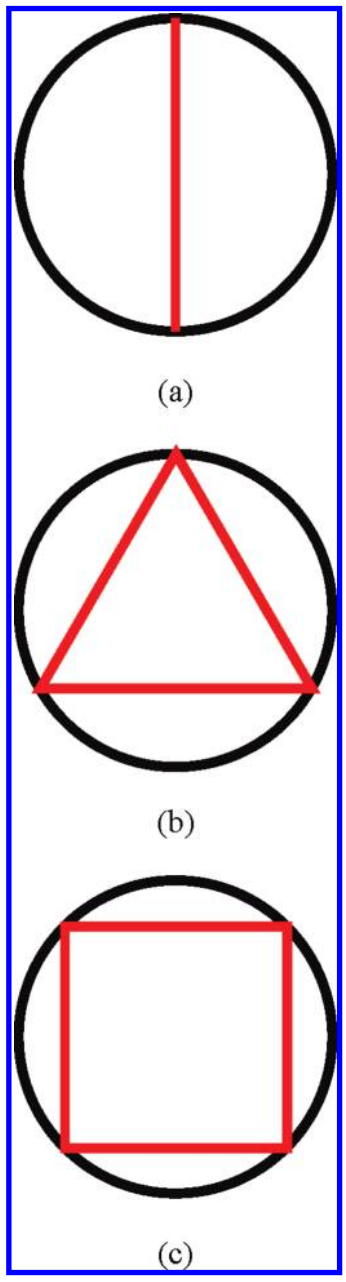

Figure 13. The schematic pictures of domain distribution corresponding to morphologies: (a) r2, (b) r3, (c) r4, respectively. The outer circle and inner lines represent the boundary of the pore and the geometric distribution of one component, respectively.

via the combination of confinement effect and the complex chain architecture. Considering the complexity of the parameter space in star polymers, more novel morphologies can be expected by tuning chain architecture and interaction potential.

Acknowledgment. This work is supported by the National Natural Science Foundation of China (20774096, 50973110, 20804047) Programs and the Fund for Creative Research Groups (50921062), and subsidized by the Special Funds for National Basic Research Program of China (2009CB930100).

References and Notes

(1) Bates, F. S.; Fredrickson, G. H. *Phys. Today* **1999**, *52*, 32–38.
(2) Hajduk, D. A.; Takenouchi, H.; Hillmyer, M. A.; Bates, F. S.; Vigild, M. E.; Almdal, K. *Macromolecules* **1997**, *30*, 3788–3795.
(3) Park, C.; Yoon, J.; Thomas, E. L. *Polymer* **2003**, *44*, 6725–6760.
(4) Yu, B.; Sun, P.; Chen, T.; Jin, Q.; Ding, D.; Li, B.; Shi, A.-C. *Phys. Rev. Lett.* **2006**, *96*, 138306.
(5) Feng, J.; Ruckenstein, E. *J. Chem. Phys.* **2007**, *126*, 124902.
(6) Binder, K. *Adv. Polym. Sci.* **1994**, *138*, 1.
(7) Binder, K.; Müller, M. *Curr. Opin. Colloid Interface Sci.* **2000**, *5*, 314–322.
(8) Fasolka, M. J.; Mayes, A. M. *Annu. Rev. Mater. Sci.* **2001**, *31*, 323–355.
(9) Shin, K.; Xiang, H.; Moon, S. I.; Kim, T.; McCarthy, T. J.; Russell, T. P. *Science* **2004**, *306*, 76–76.
(10) Xiang, H.; Shin, K.; Kim, T.; Moon, S. I.; McCarthy, J. T.; Russell, T. P. *Macromolecules* **2004**, *37*, 5660–5664.
(11) Xiang, H.; Shin, K.; Kim, T.; Moon, S. I.; McCarthy, T. J.; Russell, T. P. *J. Polym. Sci., Part B: Polym. Phys.* **2005**, *43*, 3377–3383.
(12) Xiang, H.; Shin, K.; Kim, T.; Moon, S. I.; McCarthy, T. J.; Russell, T. P. *Macromolecules* **2005**, *38*, 1055–1056.
(13) He, X.; Song, M.; Liang, H.; Pan, C. *J. Chem. Phys.* **2001**, *114*, 10510–10513.
(14) Chen, P.; He, X.; Liang, H. *J. Chem. Phys.* **2006**, *124*, 104906.
(15) Feng, J.; Ruckenstein, E. *Macromolecules* **2006**, *39*, 4899–4906.
(16) Feng, J.; Ruckenstein, E. *J. Chem. Phys.* **2006**, *125*, 164911.
(17) Wang, Q. *J. Chem. Phys.* **2007**, *126*, 024903.
(18) Sevink, H.J. A.; Zvelindovsky, A. V.; Fraaije, J. G. E. M.; Huinink, H. P. *J. Chem. Phys.* **2001**, *115*, 8226–8230.
(19) Li, W.; wickham, R. A.; Garbary, R. A. *Macromolecules* **2006**, *39*, 806–811.
(20) Li, W.; wickham, R. A. *Macromolecules* **2006**, *39*, 8492–8498.
(21) Chen, P.; Liang, H.; Shi, A.-C. *Macromolecules* **2007**, *40*, 7329–7335.
(22) Yu, B.; Sun, P.; Chen, T.; Jin, Q.; Ding, D.; Li, B.; Shi, A.-C. *J. Chem. Phys.* **2007**, *126*, 204903.
(23) Yu, B.; Sun, P.; Chen, T.; Jin, Q.; Ding, D.; Li, B.; Shi, A.-C. *J. Chem. Phys.* **2007**, *127*, 114906.
(24) Chen, P.; Liang, H. *J. Phys. Chem. B* **2008**, *112*, 1918–1925.
(25) Wu, Y.; Cheng, G.; Katsov, K.; Sides, S. W.; Wang, J.; Tang, J.; Fredrickson, G. H.; Moskovits, M.; Stucky, G. D. *Nat. Mater.* **2004**, *3*, 816–822.
(26) Zhu, Y.; Jiang, W. *Macromolecules* **2007**, *40*, 2872–2881.
(27) Mogi, Y.; Kotsuji, H.; Kaneko, Y.; Mori, K.; Matsushita, Y.; Noda, I. *Macromolecules* **1992**, *25*, 5408.
(28) Mogi, Y.; Mori, K.; Matsushita, Y.; Noda, I. *Macromolecules* **1992**, *25*, 5412–5415.
(29) Gido, S. P.; Schwark, D. W.; Thomas, E. L.; Goncalves, M. *Macromolecules* **1993**, *26*, 2636–2640.
(30) Zheng, W.; Wang, Z.-G. *Macromolecules* **1995**, *28*, 7215–7223.
(31) Tang, P.; Qiu, F.; Zhang, H.; Yang, Y. *Phys. Rev. E* **2004**, *69*, 031803.
(32) Fujimoto, T.; Zhang, H.; Kazama, T.; Isono, Y.; Hasegawa, H.; Hashimoto, T. *Polymer* **1992**, *33*, 2208–2213.
(33) Iatrou, H.; Hadjichristidis, N. *Macromolecules* **1992**, *25*, 4649–4651.
(34) Hadjichristidis, N.; Iatrou, H.; Behal, S. K.; Chludzinski, J. J.; Disko, M. M.; Garner, R. T.; Liang, K. S.; Lohse, D. J.; Milner, S. T. *Macromolecules* **1993**, *26*, 5812–5815.
(35) Sioula, S.; Hadjichristidis, N.; Thomas, E. L. *Macromolecules* **1998**, *31*, 5272–5277. Sioula, S.; Hadjichristidis, N.; Thomas, E. L. *Macromolecules* **1998**, *31*, 8429–8432.
(36) Huckstadt, H.; Goldacker, T.; Gopfert, A.; Abetz, V. *Macromolecules* **2000**, *33*, 3757–3761.
(37) Yamauchi, K.; Akasaka, S.; Hasegawa, H.; Istrou, H.; Hadjichristidis, N. *Macromolecules* **2005**, *38*, 8022–8027.
(38) Hayashida, K.; Kawashima, W.; Takano, A.; Shinohara, Y.; Amemiya, Y.; Nozue, Y.; Matsushita, Y. *Macromolecules* **2006**, *39*, 4869–4872.
(39) Hayashida, K.; Takano, A.; Arai, S.; Shinohara, Y.; Amemiya, Y.; Matsushita, Y. *Macromolecules* **2006**, *39*, 9402–9408.
(40) Kayashida, K.; Dotera, T.; Takano, A.; Matsushita, Y. *Phys. Rev. Lett.* **2007**, *98*, 195502.
(41) Kayashida, K.; Saito, N.; Arai, S.; Takano, A.; Tanaka, N.; Matsushita, Y. *Macromolecules* **2007**, *40*, 3695–3699.
(42) Bohbot-Raviv, Y.; Wang, Z.-G. *Phys. Rev. Lett.* **2000**, *85*, 3428–3431.
(43) Gemma, T.; Hatano, A.; Dotera, T. *Macromolecules* **2002**, *35*, 3225–3237.
(44) He, X.; Huang, H.; Liang, H.; Pan, C. *J. Chem. Phys.* **2003**, *118*, 9861–9863.
(45) Guo, Z.; Zhang, G.; Qiu, F.; Zhang, H.; Yang, Y.; Shi, A.-C. *Phys. Rev. Lett.* **2008**, *101*, 028301.
(46) Tang, P.; Qiu, F.; Zhang, H.; Yang, Y. *J. Phys. Chem. B* **2004**, *108*, 8434–8438.

(47) Huang, C.-I.; Fang, H.-K.; Lin, C.-H. *Phys. Rev. E* **2008**, *77*, 031804.
(48) Xu, Y.; Li, W.; Qiu, F.; Yang, Y.; Shi, A.-C. *J. Phys. Chem. B* **2009**, *113*, 11153–11159.
(49) Li, Y.; Huang, Q.; Shi, T.; An, L. *J. Phys. Chem. B* **2006**, *110*, 23502–23506.
(50) Reiter, J.; Edling, T.; Pakula, T. *J. Chem. Phys.* **1990**, *93*, 837–844.
(51) Carmesin, I.; Kremer, K. *Macromolecules* **1988**, *21*, 2819–2823.
(52) Deutsch, H. P.; Binder, K. *J. Chem. Phys.* **1991**, *94*, 2294–2304.
(53) Verdierand, P. H.; Stockmayer, W. H. *J. Chem. Phys.* **1962**, *36*, 227–235.
(54) Song, J.; Shi, T.; Li, Y.; Chen, J.; An, L. *J. Chem. Phys.* **2008**, *129*, 054906.
(55) Wilding, N. B.; Müller, M.; Binder, K. *J. Chem. Phys.* **1996**, *105*, 802–809.
(56) Pinna, M.; Guo, X.; Zvelindovsky, A. V. *J. Chem. Phys.* **2009**, *131*, 214902.
(57) Morita, H.; Kawakatsu, T.; Doi, M.; Yamaguchi, D.; Takenaka, M.; Hashimoto, T. *J. Phys. Soc. Jpn.* **2004**, *73*, 1371–1374.
(58) Wang, Q.; Yan, Q.; Nealey, P. F.; de Pablo, J. J. *J. Chem. Phys.* **2000**, *112*, 450–464.

JP102863W